High-resolution optical spectrum characterization using optical channel estimation and spectrum stitching technique

Chao Jin,[1] Yuan Bao,[1] Zhaohui Li,[1,*] Tao Gui,[1] Haiyan Shang,[2] Xinhuan Feng,[1] Jianping Li,[1] Xingwen Yi,[3] Changyuan Yu,[4] Guifang Li,[5,6] and Chao Lu[7]

[1]*Institute of Photonics Technology, Jinan University, Guangzhou 510632, China*

[2]*School of Information Science and Engineering, Shandong University, Jinan 250100, China*

[3]*School of Communication and Information Engineering, University of Electronic Science and Technology of China, China*

[4]*Department of Electrical and Computer Engineering, National University of Singapore, Singapore, 117576*

[5]*CREOL, University of Central Florida, Orlando, Florida 32816, USA*

[6]*Tianjin University, Tianjin, China*

[7]*Photonics Research Centre, The Hong Kong Polytechnic University, Hong Kong, China*

**Corresponding author: li_zhaohui@hotmail.com*

Received January 21, 2013; revised April 30, 2013; accepted May 8, 2013;
posted May 13, 2013 (Doc. ID 183713); published June 26, 2013

A technique is proposed to measure the high-resolution and wide-band characterization of amplitude, phase responses, and polarization property of optical components. This technique combines the optical spectrum stitching and optical channel estimation methods. Two kinds of fiber Bragg grating based Fabry–Perot cavities with ultrafine structures have been characterized based on this technique. By using 1024 point fast Fourier transform and a narrow linewidth, wavelength-tunable laser source, a frequency resolution of ~10 MHz is realized with an optical measurement range beyond 250 GHz. © 2013 Optical Society of America

OCIS codes: (120.2230) Fabry-Perot; (070.2025) Discrete optical signal processing.
http://dx.doi.org/10.1364/OL.38.002314

Ultra-high-resolution characterization of passive optical components, including their amplitude, phase responses, and polarization property, is very important for the measurement used in optical communication, optical sensing, and bio-engineering applications [1–3]. Generally, a number of techniques have been developed and are commonly used to measure the optical spectral characteristics of passive optical components. These include optical spectrum analyzer (OSA), laser scanning technique [4,5], and optical frequency domain reflectometry [6]. However, these techniques have some limitations, including low measurement resolution, low measurement speed, and inability to obtain the phase responses. These weaknesses have limited their ability to characterize the different properties of ultrafine structures of passive optical components simultaneously.

To improve the measurement resolution and speed, we recently have demonstrated a technique based on optical channel estimation (OCE) using coherent orthogonal frequency division multiplexing (OFDM) signals that can offer a high resolution of 0.732 MHz [7]. More importantly, no scanning is needed to obtain the amplitude and phase responses of the component, but the maximum measurable frequency range is limited within 12 GHz and polarization characterization is not involved.

In this paper, based on our previous work [7–9], we propose a technique to significantly increase the measurement range to enable the realization of high-resolution and wide band characterization of optical components using optical spectrum stitching (OSS) and OCE techniques (OCE–OSS for brevity). This technique has enabled successful characterization of the amplitude and phase responses, as well as polarization property, of fiber Bragg grating (FBG)-based Fabry–Perot (FP) cavities that are widely used in fiber lasers [10] and fiber sensor systems [11]. The experimental results also show that this technique can achieve ultrafine and wide-band measurement of optical components.

The experimental setup of OCE–OSS technique and the digital signal processing (DSP) module are shown in Fig. 1. A narrow linewidth (<100 kHz) and high wavelength accuracy (<3 pm) tunable laser source (TLS) is used to scan over a wavelength range of interest. Its output is split into two branches by a polarization maintaining (PM) splitter; one is fed into a Mach–Zehnder modulator (MZM) to generate the optical OFDM signal and another enters directly into the coherent receiver as the local oscillator (LO) laser. The measurement path includes an erbium-doped fiber amplifier (EDFA), an optical circulator, and the device under test (DUT). The electric OFDM signal is generated by an arbitrary waveform generator (AWG) at 11 GS/s. Then it is amplified by an electronic driver and modulated onto an

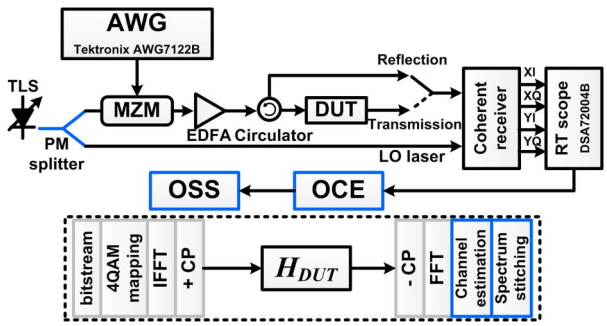

Fig. 1. Diagram of experimental setup and DSP module. IFFT, inverse fast Fourier transform (FFT); CP, cyclic prefix.

optical carrier through the MZM biased at null point. After experiencing the measurement path and coherent detection, the OFDM signal is digitalized by a real-time oscilloscope operated at 25 GS/s. Then the OFDM-based OCE technique is employed to obtain the high-resolution optical responses of DUT. Since this technique is based on coherent detection with the same signal and LO laser, it is immune to the polarization sensitivity induced by environmental instabilities and can compensate automatically the phase error due to laser tuning.

The principle of the OCE technique is described as follows. We assume that the electrical field of optical OFDM signals, before and after passing through DUT, have the form of

$$E_{\text{in}}(t) = \sum_{n=N_{\text{FFT}}/2}^{N_{\text{FFT}}/2-1} \frac{H_{B2B}(n)T(n)e^{j2\pi\Delta f nt}E_0(t)}{R_{B2B}(n)}$$
$$E_{\text{out}}(t) = \sum_{n=N_{\text{FFT}}/2}^{N_{\text{FFT}}/2-1} \frac{H_{B2B}(n)H_{\text{DUT}}(n)T(n)e^{j2\pi\Delta f nt}E_0(t)}{R_{\text{DUT}}(n)}, \quad (1)$$

where $T(n)$ is the transmitted symbol on the nth subcarrier and $E_0(t)$ is the optical carrier. $R_{B2B}(n)$ and $R_{\text{DUT}}(n)$ represent the received symbols without and with DUT, respectively. Subcarrier spacing $\Delta f = f_{\text{AWG}}/N_{\text{FFT}}$ is also referred to as the measurement resolution, where f_{AWG} is the sampling rate of the AWG and N_{FFT} is the number of FFT point. Note that the higher resolution can be achieved by using a larger point FFT. Then the responses of DUT can be obtained as $H_{\text{DUT}}(n) = E[R_{\text{DUT}}(n)/T(n)]/E[R_{B2B}(n)/T(n)]$, where $E(\bullet)$ is the expectation. To improve measurement accuracy, the 4-ary quadrature amplitude modulation (4 QAM) format is applied on each subcarrier due to its low peak to average power ratio. Here we choose a 1024-point FFT to achieve a frequency resolution of 10.7 MHz by considering the influence of phase noise of laser and measurement speed. However, if OCE is used alone, measurement range is significantly limited by the bandwidth of the OFDM signal generated by the AWG. Here we propose the use of the OSS technique to obtain the wide range responses of the DUT at different wavelengths.

To overcome the limitation of measurement range, TLS is used to shift the center wavelength of the OCE observing window, $E_0(t)$. OSS technique is then needed, as illustrated in Fig. 2, to combine all the measured responses automatically. In the experiment, the swept step size of the TLS is set at 10 GHz. The desired optical response of DUT can be divided into several segments with an OCE bandwidth of 11 GHz each and 1 GHz overlap between the neighboring segments. We assume that

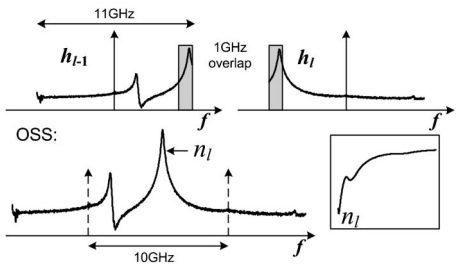

Fig. 2. Graphical representation of the OSS technique.

the separate amplitude responses are $\{\boldsymbol{h_1}\}, \{\boldsymbol{h_2}\}, \ldots, \{\boldsymbol{h_l}\}$ and $\boldsymbol{h_l} = 10\log_{10}|\boldsymbol{H_{DUT,l}}|$. The stitching point of the lth segment can be estimated by

$$n_l = \arg\min_n \sum_{i=0}^{L-1} |h_{l-1}(N_{\text{FFT}}/2 - L + i) - h_l(n - L + i)|, \quad (2)$$

where L is the overlap length between segments $\{\boldsymbol{h_{l-1}}\}$ and $\{\boldsymbol{h_l}\}$. The estimated stitching point can also be used to monitor the wavelength shift between two successive measurements to ensure the wavelength adjustment satisfies the 10 GHz channel spacing requirement. Here, we use the amplitude response alone to estimate the stitching point since the phase response of each segment suffers from random phase drift when wavelength tunes.

The proof-of-concept experiment is implemented to characterize two kinds of FBG-based FP cavities that are fabricated by inscribing a pair of FBGs in PM erbium-doped fiber (EDF). The first one is with 3.5 and 4.7 mm lengths of high- and low-reflection gratings, respectively. The length of FP cavity is 5 mm. The transmission and reflection spectra measured by an OSA (YOKOGAWA AQ6370B) are shown in Fig. 3(a). The corresponding fine amplitude responses measured by the OCE–OSS technique are shown in Fig. 3(b) for comparison. From Fig. 3(b), it can be seen that, except the original resonant peaks marked as P1 and P2, a new peak marked as P3 has been found. The 1 and 5 dB bandwidth of P3 measured using the OCE–OSS technique is about 21.4 and 96.3 MHz (<100 MHz), respectively. Such a fine structure obviously cannot be observed by ordinary OSAs.

To further verify the advantages of the proposed technique, another FBG-based active FP cavity etched in PM–EDF with 6 mm high- and low-reflection gratings,

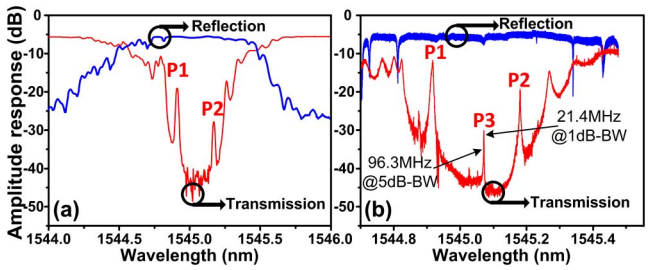

Fig. 3. The measured transmission and reflection spectra of the first FP cavity by (a) OSA and (b) OCE–OSS technique.

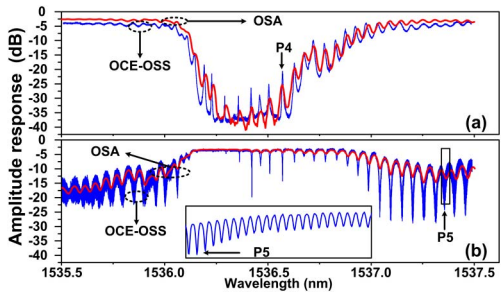

Fig. 4. Measurement results of the second FP cavity by OCE–OSS (blue) and OSA (red) on (a) transmission and (b) reflection.

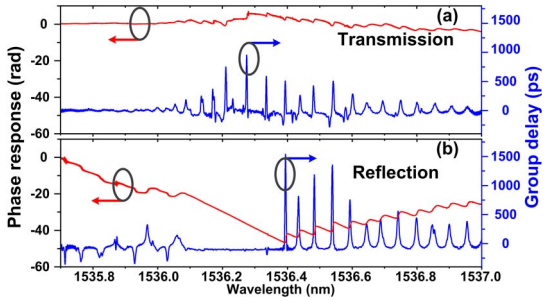

Fig. 5. Measured phase response and group delay on (a) transmission and (b) reflection of the FBG-based FP cavity.

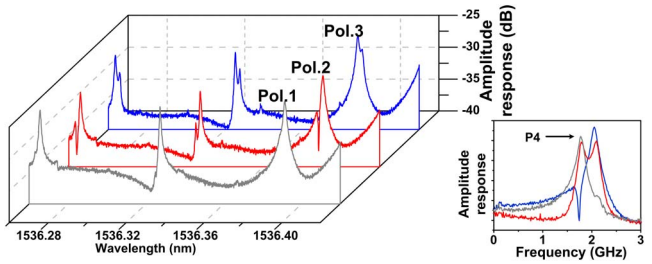

Fig. 6. Polarization properties of resonant peaks of FP cavity.

and a 15 mm active cavity that means a more fine spectrum, has been measured. Figures 4(a) and 4(b) show the transmission and reflection spectra measured by OSA (red line) and OCE–OSS (blue line) techniques respectively. It can be seen that the amplitude response measured, based on the two techniques, are almost consistent with each other within 2 nm (250 GHz). That means the measurement range has been successfully extended by the proposed OSS technique. Moreover, the resonant peak marked as P4 in Fig. 4(a) with an actual frequency spacing just 310 MHz (2.46 pm) can be observed by OCE–OSS technique, whereas it is almost impossible to be distinguished by OSAs. Additionally, some new deep optical spectrum notches can also be observed based on OCE–OSS. These notches are originated from the multiple interference of the signals reflected by different FBG etched in the PM fiber, e.g., P5 in Fig. 4(b). The inset shows the fine structures of these notches in detail. Nevertheless, there are few defects about this proposed technique as shown in Fig. 4. This is likely due to the phase change of the DUT caused by environment change during the TLS tuning since the tuning and measurement was done manually during the experiment. These defects will disappear when the automatic measurement process is adopted. The limited linear response region of the coherent receiver does not influence its feasibility.

Furthermore, the wide-band phase response of the DUT can also be obtained by the OCE–OSS technique. To correct the TLS tuning-induced phase drift, an automatic phase stitching algorithm is adopted, and described as follows. We first unwrap the phase response of each segment as $\{\boldsymbol{p_1}\}, \{\boldsymbol{p_2}\}, \ldots, \{\boldsymbol{p_l}\}$. Then we obtain the differential phase by $\Delta p_l(n) = p_l(n+1) - p_l(n)$. We stitch the differential results $\{\boldsymbol{\Delta p_l}\}$ with the same stitching point n_l to obtain the full span of $\{\boldsymbol{\Delta p}\}$, and the final phase response is achieved by summing up the differential phases as $\tilde{p}(m) = \sum_{i=1}^{m} \Delta p(i)$, and then the group delay can also be obtained as $\tau(m) = \Delta p(m)/(2\pi\Delta f)$.

Figure 5 shows the measured phase response and group delay on transmission and reflection of the second FBG-based FP cavity. Obviously, the optical signal experiences large group delay if its wavelength matches the resonant cavity. The transmission group delay seems a little noisier than reflection since the transmitted signal is weaker than the reflected one.

Another feature of this technique is that the polarization property of components can also be studied as shown in Fig. 6. As can be seen from the figure, when the state of polarization (SOP) of the input optical signal is changed, characteristics of resonant peaks will also change accordingly. Inset shows a very typical example, which is the detail of resonant peak P4 as shown in Fig. 4(a). Actually two peaks in P4 can be distinguished and either one may disappear dramatically during the SOP variation due to their polarization property. There would be no doubt that this feature is useful in some special applications where high-resolution polarization characteristics are an important concern.

In conclusion, the ultrafine optical spectrum structure of an FBGbased FP cavity has been successfully characterized based on the OCE–OSS technique. The results show that the proposed technique not only enables high-resolution measurement of amplitude and phase responses over a wide wavelength range, but also allows the polarization properties to be characterized.

The authors would like to acknowledge the support of National Basic Research Programme of China project (No.2012CB315603) and the Program for New Century Excellent Talents in University (NCET-12-0679) in China.

References

1. W. J. Tomlinson, J. Lightwave Technol. **26**, 1046 (2008).
2. D. C. Adler, Y. Chen, R. Huber, J. Schmitt, J. Connolly, and J. G. Fujimoto, Nat. Photonics **1**, 709 (2007).
3. I. Coddington, W. C. Swann, L. Nenadovic, and N. R. Newbury, Nat. Photonics **3**, 351 (2009).
4. B. J. Soller, D. K. Gifford, M. S. Wolfe, and M. E. Froggatt, Opt. Express **13**, 666 (2005).
5. G. D. VanWiggeren, A. R. Motamedi, and D. M. Baney, IEEE Photon. Technol. Lett. **15**, 263 (2003).
6. R. C. Youngquist, S. Carr, and D. E. N. Davies, Opt. Lett. **12**, 158 (1987).
7. X. Yi, Z. Li, Y. Bao, and K. Qiu, IEEE Photon. Technol. Lett. **24**, 443 (2012).
8. B. Guo, T. Gui, Z. Li, Y. Bao, X. Yi, J. Li, X. Feng, and S. Liu, Opt. Express **20**, 22079 (2012).
9. H. Shang, Z. Li, T. Gui, Y. Bao, X. Feng, J. Li, H. Fu, and D. Geng, in *Optical Fiber Communications Conference* (Optical Society of America, 2013), paper OW4H.4.
10. W. Guo, D. Byrne, Q. Lu, B. Corbett, and J. F. Donegan, IEEE J. Sel. Top. Quantum Electron. **17**, 1356 (2011).
11. J. Zhang, Q. Sun, R. Liang, J. Wo, D. Liu, and P. Shum, Opt. Lett. **37**, 2925 (2012).